Generalized Laplacian Eigenmaps

Hao Zhu[†,§] **Piotr Koniusz**[*,§,†]
[§]Data61/CSIRO [†]Australian National University
allenhaozhu@gmail.com, piotr.koniusz@data61.csiro.au

Abstract

Graph contrastive learning attracts/disperses node representations for similar/dissimilar node pairs under some notion of similarity. It may be combined with a low-dimensional embedding of nodes to preserve intrinsic and structural properties of a graph. COLES, a recent graph contrastive method combines traditional graph embedding and negative sampling into one framework. COLES in fact minimizes the trace difference between the within-class scatter matrix encapsulating the graph connectivity and the total scatter matrix encapsulating negative sampling. In this paper, we propose a more essential framework for graph embedding, called Generalized Laplacian EigeNmaps (GLEN), which learns a graph representation by maximizing the rank difference between the total scatter matrix and the within-class scatter matrix, resulting in the minimum class separation guarantee. However, the rank difference minimization is an NP-hard problem. Thus, we replace the trace difference that corresponds to the difference of nuclear norms by the difference of LogDet expressions, which we argue is a more accurate surrogate for the NP-hard rank difference than the trace difference. While enjoying a lesser computational cost, the difference of LogDet terms is lower-bounded by the Affine-invariant Riemannian metric (AIRM) and upper-bounded by AIRM scaled by the factor of $\sqrt{m}$. We show on popular benchmarks/backbones that GLEN offers favourable accuracy/scalability compared to state-of-the-art baselines.

1 Introduction

Laplacian Eigenmaps [3] and IsoMap [39] are graph embedding methods that reduce the dimensionality of data by assuming the data exists on a low-dimensional manifold. The objective function in such models encourages node embeddings to lie near each other in the embedding space if nodes are close to each other in the original space. While the classical methods capture the related node pairs, they neglect modeling unrelated node pairs.

In contrast, modern graph embedding models such as [38, 10, 47] and Graph Contrastive Learning (GCL) [40, 63, 11, 64, 62] are unified under the (Sampled) Noise Contrastive Estimation framework, called (Sampled)NCE [28, 23]. Most of GCL methods do not incorporate the graph information into the loss but follow the setting from computer vision, *i.e.*, they assume that randomly drawn pairs should be dissimilar, whereas the original sample and its augmentations should be similar [42]. In contrast, COntrastive Laplacian EigenmapS (COLES) [62] is a framework which combines a (graph) neural network with Laplacian eigenmaps utilizing the graph Laplacian matrix within a contrastive loss. Based on the NCE framework, COLES minimizes the trace difference of Laplacians.

In this paper, we analyze the relation among within-class, between-class and total scatter matrices under the rank inequality, and prove that, under a simple assumption, the distance between any dissimilar (negative) samples would be greater/equal than the inter-class distance between their corresponding class centers. Based on such a condition, we derive GLEN, a reformulation of graph embedding into a rank difference problem, which is a more general framework than other graph

[*]The corresponding author. Code: `https://github.com/allenhaozhu/GLEN`.

36th Conference on Neural Information Processing Systems (NeurIPS 2022).

embedding frameworks, *i.e.*, under specific relaxations of the rank difference problem, we can recover different frameworks.To that end, we demonstrate how to optimize the rank difference problem with a difference of LogDet expressions, a differentiable relaxation suitable for use with (graph) neural networks. We consider other surrogates of the rank difference problem, based on the Nuclear norm, γ-nuclear norm, Schatten norm, and the Geman norm. Moreover, we provide theoretical considerations regarding the low-rank optimization and connection to the Riemannian manifold in order to interpret our approach.

In summary, our contributions are threefold:

i. We propose a rank-based condition connecting within-class, between-class and total scatter matrices under which we provide the minimum class separation guarantee. We propose a loss function, Generalized Laplacian EigenNaps (GLEN), that realizes this condition.

ii. As the rank difference problem is NP-hard, we consider a difference of LogDet surrogate to learn node embeddings, as opposed to the trace difference (an upper bound of the difference of LogDet terms) used by other graph embedding models. We also consider other surrogates.

iii. We study the distance between symmetric positive (semi-)definite matrices and the LogDet-based relaxation of GLEN. While enjoying fewer computations, the difference of LogDet terms of GLEN enjoys the Affine-invariant Riemannian metric (AIRM) for a lower bound and AIRM scaled by $\sqrt{m}$ as an upper bound. We explain how GLEN connects to other graph embeddings.

2 Related Works

Graph Embeddings. By assuming that the data lies on a low-dimensional manifold, graph embedding methods such as Laplacian Eigenmaps [3] and IsoMap [39] optimize low-dimensional data embeddings. These methods [5] construct a similarity graph by measuring the similarity of high-dimensional feature vectors and embed the nodes into a low-dimensional space.

DeepWalk [32] uses truncated random walks to explore the graph structure, and the skip-gram model for word embedding to determine the embedding vectors of nodes. By setting the walk length to one and using negative sampling [27], LINE [38] explores a similar idea with an explicit objective function while REFINE [59] imposes additional orthogonality constraints which deem REFINE extremely fast. Node2Vec [9] interpolates between breadth- and depth-first sampling. COLES [62] unifies traditional graph embedding and negative sampling by introducing a positive contrastive term that captures the graph structure, and a negative contrastive random sampling. COLES solves the trace difference problem akin to traditional graph embedding models [46]. In this paper, we propose a more general loss for graph embedding, *i.e.*, COLES solves the trace difference (Nuclear norms difference) relaxation of GLEN.

Graph embedding techniques [46] provide a general framework for dimensionality reduction such as Principal Component Analysis (PCA), Linear Discriminant Analysis (LDA), and Locality Preserving Projections (LPP) [12]. All methods within this category can be considered as solving the same problem under varying assumptions, *i.e.*, maximising the intra- and inter-class separation by optimizing the trace difference, also used in metric learning [22]. However, such a family of objective functions is not motivated by the guarantee on the minimum class separation between feature vectors from different categories. GLEN, in its purest NP-hard form, provides the minimum class separation guarantee and can be realised by several formulations depending on chosen trade-offs.

Unsupervised Representation Learning for Graph Neural Networks (GNN). Unsupervised GNN training can be reconstruction-, contrastive- or diffusion-based. To train a graph encoder in an unsupervised manner, GCN [17] minimizes a reconstruction error which only considers the similarity matrix and ignores the dissimilarity information. At various scales of the graph, contrastive methods determine the positive and negative sets. For example, local-local CL and global-local CL strategies are highly popular. GraphSAGE [10], inspired by DeepWalk [32], uses the contrastive loss which encourages neighbor nodes to have similar representations, while preserving dissimilarity between representations of disparate nodes. DGI [40], inspired by Deep InfoMax (DIM) [13], uses an objective with global-local sampling strategy to maximize the Mutual Information (MI) between global and local graph embeddings. Augmented Multiscale Deep InfoMax (AMDIM) [2] maximizes MI between multiple data views. MVRLG [11] contrasts encodings from first-order neighbors and a graph diffusion. Fisher-Bures Adversary GCN [36] treats the graph as generated w.r.t. some observation noise. COSTA [57] constructs the views by injecting features with the random noise.

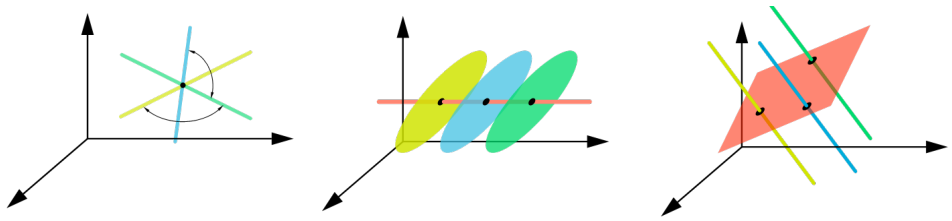

(a) $\mathrm{Rank}(S_b) = 0$ (b) $\mathrm{Rank}(S_b) = 1$ (c) $\mathrm{Rank}(s_b) = 2$

Figure 1: Three cases under our Condition 1, *i.e.*, $\mathrm{Rank}(\mathbf{S}_t) = \mathrm{Rank}(\mathbf{S}_w) + \mathrm{Rank}(\mathbf{S}_b)$. The red line and plane indicate the space of class centers. The black dots represent class centers. Other colored lines or ellipses represent the spaces of different categories. We show a non-exhaustive set of cases.

However, such contrastive approaches often require thousands of epochs to converge and perform well. In addition, many contrastive losses have an exponential increase in memory overhead w.r.t. the number of nodes. In contrast, our method does not explicitly use the local-local setting but the total scatter matrix, and thus saves computational and storage cost.

Linear GNNs, *i.e.*, SGC [45] and S^2GC [60], capture the neighborhood and increasingly larger neighborhoods of each node due to the diffusion, respectively. SGC and S^2GC have no projection layer, thus the size of embeddings is equal to the input dimension. GLEN can learn a projection layer in an unsupervised manner with a linear function or Multi-Layer Perceptron (MLP) applied to linear GNNs or any other GNN models [18, 36, 56], *etc*.

3 Preliminaries

Notations. Let $G = (V, E)$ be a simple, connected and undirected graph with $n = |V|$ nodes and $m = |E|$ edges. Let $i \in \{1, \cdots, n\}$ be the node index of G, and d_j be the degree of node j of G. Let $\mathbf{W}$ be the adjacency matrix, and $\mathbf{D}$ be the diagonal matrix containing degrees of nodes. Let $\mathbf{X} \in \mathbb{R}^{n \times d}$ denote the node feature matrix where each node v is associated with a feature vector $\mathbf{x}_v \in \mathbb{R}^d$. Let the normalized graph Laplacian matrix be defined as $\mathbf{L} = \mathbf{I} - \tilde{\mathbf{W}} \in \mathbb{S}_+^n$, a symmetric positive semi-definite matrix and $\tilde{\mathbf{W}} = \mathbf{D}^{-1/2}\mathbf{W}\mathbf{D}^{-1/2}$. $\mathbb{S}_{+(+)}^m$ is a set of symmetric positive (semi-)definite matrices. Let $\mathbf{Z} = f_{\boldsymbol{\Theta}}(\mathbf{X}) \in \mathbb{R}^{n \times m}$ be a generalized node embedding, *i.e.*, $\mathbf{X}$ could be identity matrix (*e.g.*, no node attributes), $f_{\boldsymbol{\Theta}}(\mathbf{X})$ could be GNN or a linear function with parameters $\boldsymbol{\Theta}$. Scalars/vectors/matrices are denoted by lowercase regular/lowercase bold/uppercase bold fonts.

3.1 Scatter Matrices

Below are given standard definitions of scatter matrices, including the total scatter matrix $\mathbf{S}_t \in \mathbb{S}_{+(+)}^m$, the within-class matrix $\mathbf{S}_w \in \mathbb{S}_{+(+)}^m$, and between-class matrix $\mathbf{S}_b \in \mathbb{S}_{+(+)}^m$:

$$\begin{aligned}
\mathbf{S}_t &= \sum_{i=1}^{n} (\mathbf{z}_i - \bar{\mathbf{z}})(\mathbf{z}_i - \bar{\mathbf{z}})^\top = \mathbf{Z}^\top(\mathbf{I} - \tilde{\mathbf{W}}_t)\mathbf{Z} \qquad \text{where} \quad \tilde{\mathbf{W}}_t = \frac{1}{n}\mathbf{e}\mathbf{e}^\top, \\
\mathbf{S}_w &= \sum_{i=1}^{n} (\mathbf{z}_i - \boldsymbol{\mu}_{y_i})(\mathbf{z}_i - \boldsymbol{\mu}_{y_i})^\top = \mathbf{Z}^\top(\mathbf{I} - \tilde{\mathbf{W}}_w)\mathbf{Z} \quad \text{where} \quad \tilde{\mathbf{W}}_w = \sum_{c=1}^{C} \frac{1}{n_c}\mathbf{e}^c\mathbf{e}^{c\top}, \\
\mathbf{S}_b &= \sum_{c=1}^{C} n_c (\boldsymbol{\mu}_c - \bar{\mathbf{z}})(\boldsymbol{\mu}_c - \bar{\mathbf{z}})^\top. \qquad (1)
\end{aligned}$$

Let $\mathbf{e}$ be an n-dimensional vector with all coefficients equal one, $\mathbf{I}$ be an identity matrix, $\mathbf{S}_t$ be the total scatter (covariance) matrix, and $\bar{\mathbf{z}} \in \mathbb{R}^m$ be the mean of all samples. Let $\boldsymbol{\mu}_{y_i} \in \mathbb{R}^m$ be the class center of the i-th sample and $\boldsymbol{\mu}_c \in \mathbb{R}^m$ be the c-th class center. Let the total number of categories be given by C, whereas n_c be the number of samples for the c-th category. Let $\mathbf{e}^c \in \mathbb{R}^n$ be a vector where a given coefficient indexed by node is equal one if its node is of class c, otherwise it is equal zero. We note that both $\mathbf{S}_t$ and $\mathbf{S}_w$ can take a form akin to Laplacian eigenmaps such that $\tilde{\mathbf{W}}_t$ and $\tilde{\mathbf{W}}_w$ are the corresponding normalized adjacent matrices. Let us also define graph Laplacian matrices

$\mathbf{L}_t = \mathbf{I} - \tilde{\mathbf{W}}_t \in \mathbb{S}_+^n$ and $\mathbf{L}_w = \mathbf{I} - \tilde{\mathbf{W}}_w \in \mathbb{S}_+^n$ which will be used in the sequel. Importantly, let us assume that a graph Laplacian matrix $\mathbf{L}$ containing graph links could be seen as a noisy version of $\mathbf{L}_w$ in which all nodes of a given class c connect under the weight equal $1/n_c$.

Observe that $\mathbf{S}_t = \mathbf{S}_w + \mathbf{S}_b$. Thus, $\text{Rank}(\mathbf{S}_t) \leq \text{Rank}(\mathbf{S}_w) + \text{Rank}(\mathbf{S}_b)$ due to the rank inequality. Below we highlight the condition underpinning the subsequent motivation:

Condition 1. $\text{Rank}(\mathbf{S}_t) = \text{Rank}(\mathbf{S}_w) + \text{Rank}(\mathbf{S}_b)$.

3.2 Motivation

Figure 1 shows some three optimal solutions for Condition 1. The rank of between-class scatter matrix $\mathbf{S}_b$ for the whole dataset is at most $C-1$ (where C is the number of classes). Since $\text{Rank}(AB) \leq \min(\text{Rank}(A), \text{Rank}(B))$, we have[†] $\text{Rank}(\mathbf{S}_w^{-1}\mathbf{S}_b) \leq \text{Rank}(\mathbf{S}_b) \leq C-1$. The rank is the number of non-zero eigenvalues of a matrix so $\mathbf{S}_w^{-1}\mathbf{S}_b$ has at most $C-1$ non-zero eigenvalues. Condition 1 implies that $\text{Rank}(\mathbf{S}_w^{-1}\mathbf{S}_b) = 0$ results in the minimum class separation guarantee under that condition.

Theorem 1. *Let the feature dimension be larger than the class number (*i.e.*, $m > C$) and Condition 1 hold. Then, the minimum class separation is equal to the distance between class centers. In other words, the distance between any two vectors $\mathbf{z}_i$ and $\mathbf{z}_j$ with labels $y_i \neq y_j$ is greater/equal the distance between class centers $\boldsymbol{\mu}_{y_i}$ and $\boldsymbol{\mu}_{y_j}$:*

$$\|\boldsymbol{\mu}_{y_i} - \boldsymbol{\mu}_{y_j}\|_2 \leq \|\mathbf{z}_i - \mathbf{z}_j\|_2, \ \forall y_i \neq y_j, \ i, j \in \{1, \cdots, C\}. \tag{2}$$

Proof. As $\mathbf{S}_w$ is the orthogonal complement of $\mathbf{S}_b$, *i.e.*, $\mathbf{S}_w^{-1}\mathbf{S}_b = \mathbf{0}$, $\mathbf{S}_w + \mathbf{S}_b = \mathbf{U}\Sigma\mathbf{U}^\top$, $\mathbf{S}_w = \mathbf{U}_{1:k}\Sigma_{1:k}\mathbf{U}_{1:k}^\top$ and $\mathbf{S}_b = \mathbf{U}_{k+1:m}\Sigma_{k+1:m}\mathbf{U}_{k+1:m}^\top$ where $1 \leq k < m$. Let $\mathbf{z}_i = \boldsymbol{\mu}_{y_i} + \mathbf{U}^\top\boldsymbol{\epsilon}_i$ where $\boldsymbol{\epsilon}_i$ is the representation under the basis $\mathbf{U}$ and $\boldsymbol{\epsilon}_{(k+1:m),i} = \mathbf{0}$ because only top k components $1:k$ represent $\mathbf{S}_w$. Thus, the orthogonal projection $\mathbf{U}_{k+1:m}$ fulfills $\|\mathbf{U}_{k+1:m}(\mathbf{z}_i - \mathbf{z}_j)\|_2 \leq \|\mathbf{z}_i - \mathbf{z}_j\|_2$. Moreover, $\mathbf{U}_{k+1:m}(\mathbf{z}_i - \boldsymbol{\mu}_{y_i}) = \mathbf{U}_{k+1:m}(\mathbf{U}^\top\epsilon_i) = 0$. That is, all $\{\mathbf{z}_i : y_i = c\}$ are projected onto the mean $\boldsymbol{\mu}_c$. Thus, the inequality in Eq. 2 holds. □

Theorem 1 guarantees the worst inter-class distance[§]. Figure 1 shows some cases that meet Condition 1. Figure 1a shows the case for which the class centers collapse to a single point and thus the inter-class distance equals zero (collapse of the feature space). Figures 1b and 1c show other cases.

4 Methodology

Condition 1 points to a promising research direction in learning discriminative feature spaces. However, optimizing over the rank is NP-hard and non-differentiable. In what follows, we provide the formulation of Generalized Laplacian EigeNmaps (GLEN) and its relaxation, which is differentiable.

4.1 Generalized Laplacian Eigenmaps

As solving Condition 1 is NP-hard, we propose a relaxation where $\text{Rank}(\mathbf{S}_t)$ is encouraged to be as large as possible (bounded by the feature dimension m). On the contrary, if $\text{Rank}(\mathbf{S}_t) \approx \text{Rank}(\mathbf{S}_b)$ then the small $\text{Rank}(\mathbf{S}_w)$ limits the feature diversity. In the extreme case, if $\text{Rank}(\mathbf{S}_w) = 0$, the feature representation collapses. Larger $0 < \text{Rank}(\mathbf{S}_b) \leq C-1$ improves the inter-class diversity.

We propose a new **Generalized Laplacian EigeNmaps (GLEN)** framework for unsupervised network embedding. In the most general form, GLEN maximizes the difference of rank terms:

$$\boldsymbol{\Theta}^* = \arg\max_{\boldsymbol{\Theta}} \ \text{Rank}\left(\mathbf{S}_t\left(f_{\boldsymbol{\Theta}}(\mathbf{X})\right)\right) - \text{Rank}\left(\mathbf{S}_w\left(f_{\boldsymbol{\Theta}}(\mathbf{X})\right)\right). \tag{3}$$

As the general matrix Rank Minimization Problem (RMP) [7] is NP-hard and so is the difference of rank terms in Eq. 3, we relax this problem by the difference of LogDet terms that serve as a surrogate of the NP-hard problem. Appendix H derives GLEN from the SampledNCE framework.

[†]We write $\mathbf{S}_w^{-1}$ but if $\mathbf{S}_w$ is rank-deficient, $^{-1}$ is replaced with the Moore–Penrose inverse (pseudo-inverse).

[§]Other graph embedding models that maximize/minimize inter-/intra-class distances have no such guarantees.

GLEN (LogDet relaxation).

I. Define:

$$\delta(\mathbf{S}_t, \mathbf{S}_w; \alpha, \lambda) = \log\det(\mathbf{I} + \alpha\mathbf{S}_t) - \lambda \log\det(\mathbf{I} + \alpha\mathbf{S}_w), \tag{4}$$

where $\lambda \geq 0$ controls the impact of $\log\det(\mathbf{S}_w)$. If $\lambda = 0$, $\delta(\cdot)$ encourages $\mathrm{Rank}(f_{\boldsymbol{\Theta}}(\mathbf{X})) = m$.

II. Let $\mathbf{S}_t = f_{\boldsymbol{\Theta}}(\mathbf{X})^\top \mathbf{L}_t f_{\boldsymbol{\Theta}}(\mathbf{X})$ and $\mathbf{S}_w = f_{\boldsymbol{\Theta}}(\mathbf{X})^\top \mathbf{L}_w f_{\boldsymbol{\Theta}}(\mathbf{X})$. Then the LogDet relaxation becomes:

$$\boldsymbol{\Theta}^* = \arg\max_{\boldsymbol{\Theta}} \ \log\det\left(\mathbf{I} + \alpha f_{\boldsymbol{\Theta}}(\mathbf{X})^\top \mathbf{L}_t f_{\boldsymbol{\Theta}}(\mathbf{X})\right) - \log\det\left(\mathbf{I} + \alpha f_{\boldsymbol{\Theta}}(\mathbf{X})^\top \mathbf{L}_w f_{\boldsymbol{\Theta}}(\mathbf{X})\right), \tag{5}$$

where $\mathbf{I}$ ensures $\mathbf{I} + \alpha f_{\boldsymbol{\Theta}}(\mathbf{X})^\top \mathbf{L} f_{\boldsymbol{\Theta}}(\mathbf{X}) > 0$ as $f_{\boldsymbol{\Theta}}(\mathbf{X})^\top \mathbf{L} f_{\boldsymbol{\Theta}}(\mathbf{X})$ may be $\mathbb{S}_+^m$ leading to $\det(f_{\boldsymbol{\Theta}}(\mathbf{X})^\top \mathbf{L} f_{\boldsymbol{\Theta}}(\mathbf{X})) = 0$. Thus, we use $\log\det(\mathbf{I} + \alpha\mathbf{S})$ as a smooth surrogate for $\mathrm{Rank}(\mathbf{S})$.

Proposition 1. *Let $\sigma(\mathbf{S})$ be the vector of eigenvalues of matrix $\mathbf{S} \in \mathbb{S}_{+(+)}^m$, and $\mathrm{Eig}(\mathbf{S})$ be a diagonal matrix with $\sigma(\mathbf{S})$ as its diagonal. Let $\mathbf{S}, \mathbf{S}' \in \mathbb{S}_{+(+)}^m$ and $\alpha > 0$. Then, $\delta(\mathbf{S}, \mathbf{S}'; \alpha, \lambda) = \delta(\mathrm{Eig}(\mathbf{S}), \mathrm{Eig}(\mathbf{S}'); \alpha, \lambda)$,* i.e., *$\delta(\cdot)$ depends on eigenvalues rather than eigenvectors of $\mathbf{S}$ and $\mathbf{S}'$.*

Proof. The proof follows from the equality $\det(\mathbf{I} + \alpha\mathbf{S}) = \prod_i \sigma_i(\mathbf{I} + \alpha\mathbf{S}) = \prod_i (1 + \alpha\sigma_i(\mathbf{S})) = \det(\mathbf{I} + \alpha\,\mathrm{Eig}(\mathbf{S}))$. Thus $\delta(\mathbf{S}, \mathbf{S}'; \alpha, \lambda) = \log\det(\mathbf{I} + \alpha\mathbf{S}) - \lambda\log\det(\mathbf{I} + \alpha\mathbf{S}') = \log\det(\mathbf{I} + \alpha\,\mathrm{Eig}(\mathbf{S})) - \lambda\log\det(\mathbf{I} + \alpha\,\mathrm{Eig}(\mathbf{S}')) = \delta(\mathrm{Eig}(\mathbf{S}), \mathrm{Eig}(\mathbf{S}'); \alpha, \lambda)$. □

5 Theoretical Analysis

Below, we compare our approach and other methods by looking at (i) the low-rank optimization and (ii) the non-Euclidean distances between symmetric positive (semi-)definite matrices.

5.1 Nuclear Norm *vs*. LogDet for Rank Minimization

Claim 1. *COLES [62] is a convex relaxation (using the nuclear norm) of the rank difference in Eq. 3:*

$$\boldsymbol{\Theta}^* = \arg\max_{\boldsymbol{\Theta}} \mathrm{Tr}\left(f_{\boldsymbol{\Theta}}(\mathbf{X})^\top \mathbf{L}_t f_{\boldsymbol{\Theta}}(\mathbf{X})\right) - \lambda\,\mathrm{Tr}\left(f_{\boldsymbol{\Theta}}(\mathbf{X})^\top \mathbf{L}_w f_{\boldsymbol{\Theta}}(\mathbf{X})\right) \quad \textit{s.t.} \ \ \Omega(f_{\boldsymbol{\Theta}}(\mathbf{X})) = B, \tag{6}$$

where $\mathrm{Tr}\left(f_{\boldsymbol{\Theta}}(\mathbf{X})^\top \mathbf{L}_t f_{\boldsymbol{\Theta}}(\mathbf{X})\right) = \|\mathbf{S}_t\|_*$ *and* $\mathrm{Tr}\left(f_{\boldsymbol{\Theta}}(\mathbf{X})^\top \mathbf{L}_w f_{\boldsymbol{\Theta}}(\mathbf{X})\right) = \|\mathbf{S}_w\|_*$.

The nuclear norm $\|\cdot\|_*$ can be regarded as the ℓ_1 norm over singular values. As the ℓ_1 norm induces sparsity, the nuclear norm encourages sparse singular values leading to low-rank solutions. If $f_{\boldsymbol{\Theta}}(\mathbf{X})^\top f_{\boldsymbol{\Theta}}(\mathbf{X})$ is restricted to be diagonal, $\|f_{\boldsymbol{\Theta}}(\mathbf{X})^\top f_{\boldsymbol{\Theta}}(\mathbf{X})\|_* = \|\,\mathrm{Diag}\left(f_{\boldsymbol{\Theta}}(\mathbf{X})^\top f_{\boldsymbol{\Theta}}(\mathbf{X})\right)\|_1$ and the nuclear norm surrogate for the rank minimization reduces to the ℓ_1 norm surrogate for the cardinality (rank) minimization. However, for the m-dimensional embedding, the solution of trace difference lies on a subspace of dimension less than $m - 1$ [3]. Thus, the constraint $\Omega(f_{\boldsymbol{\Theta}}(\mathbf{X})) = B$ prevents the dimensional collapse, *i.e.*, $f_{\boldsymbol{\Theta}}(\mathbf{X})^\top f_{\boldsymbol{\Theta}}(\mathbf{X}) = \mathbf{I}$.

Compared with the trace-based relaxation, LogDet is more suitable for cardinality minimization as it is less sensitive to large singular values. Also, the difference of LogDet terms does not require decorrelation of features to prevent the dimensional collapse. We discuss this matter in Appendix A. In our case, the difference of LogDet terms is always bounded by the difference of trace terms as follows.

Proposition 2. *Given an embedding matrix $f_{\boldsymbol{\Theta}}(\mathbf{X}) \in \mathbb{R}^{n\times m}$, a fixed small constant $\alpha > 0$, we have the following inequality:*

$$\log\det\left(\mathbf{I} + \alpha\mathbf{S}_t\right) - \log\det\left(\mathbf{I} + \alpha\mathbf{S}_w\right) < \alpha\,\mathrm{Tr}(\mathbf{S}_t - \mathbf{S}_w). \tag{7}$$

Proof.

$$\begin{aligned} &\log\det\left(\mathbf{I}+\alpha\mathbf{S}_t\right) - \log\det\left(\mathbf{I} + \alpha\mathbf{S}_w\right) = \log\det\left(\mathbf{I}+\alpha\,\mathrm{Eig}(\mathbf{S}_t)\right) - \log\det\left(\mathbf{I} + \alpha\,\mathrm{Eig}(\mathbf{S}_w)\right) \\ &= \mathrm{Tr}\left(\log(\mathbf{I} + \alpha\,\mathrm{Eig}(\mathbf{S}_t) - \log(\mathbf{I} + \alpha\,\mathrm{Eig}(\mathbf{S}_w)\right) < \alpha\,\mathrm{Tr}(\mathbf{S}_t - \mathbf{S}_w). \end{aligned} \tag{8}$$

□

Proposition 2 is also related to the inequality $\mathrm{Rank}(\mathbf{S}) \leq \log\det(\mathbf{I} + \mathbf{S}) \leq \mathrm{Tr}(\mathbf{S})$ [7].

5.2 Distance between Symmetric Positive (Semi-)Definite Matrices.

Below, we provide a perspective on non-Euclidean distances between matrices from $\mathbb{S}^m_{+(+)}$ to compare the proposed method with other graph embeddings, *e.g.*, Laplacian Eigenmaps [3] and COLES [62]. For clarity, we also reformulate the Laplacian eigenmaps and COLES into forms in Prop. 3 and 4.

Proposition 3. *Laplacian Eigenmaps [3] method equals to maximizing the Frobenius norm:*

$$\mathbf{\Theta}^* = \arg\max_{\mathbf{\Theta}} \|f_{\mathbf{\Theta}}(\mathbf{X})f_{\mathbf{\Theta}}(\mathbf{X})^\top - \mathbf{L}_w\|_F^2, \quad s.t. \quad f_{\mathbf{\Theta}}(\mathbf{X})^\top f_{\mathbf{\Theta}}(\mathbf{X}) = \mathbf{I}. \tag{9}$$

Proposition 4. *Contrastive Laplacian Eigenmaps [62] equals to maximizing the difference of Frobenius norm terms:*

$$\mathbf{\Theta}^* = \arg\max_{\mathbf{\Theta}} \|f_{\mathbf{\Theta}}(\mathbf{X})f_{\mathbf{\Theta}}(\mathbf{X})^\top - \mathbf{L}_w\|_F^2 - \|f_{\mathbf{\Theta}}(\mathbf{X})f_{\mathbf{\Theta}}(\mathbf{X})^\top - \mathbf{L}_t\|_F^2, \ s.t. \ f_{\mathbf{\Theta}}(\mathbf{X})^\top f_{\mathbf{\Theta}}(\mathbf{X}) = \mathbf{I}. \tag{10}$$

Proof.

$$\begin{aligned}\|f_{\mathbf{\Theta}}(\mathbf{X})f_{\mathbf{\Theta}}(\mathbf{X})^\top - \mathbf{L}\|_F^2 &= \mathrm{Tr}(f_{\mathbf{\Theta}}(\mathbf{X})f_{\mathbf{\Theta}}(\mathbf{X})^\top f_{\mathbf{\Theta}}(\mathbf{X})f_{\mathbf{\Theta}}(\mathbf{X})^\top - 2f_{\mathbf{\Theta}}(\mathbf{X})\mathbf{L}f_{\mathbf{\Theta}}(\mathbf{X})^\top + \mathbf{L}^\top\mathbf{L}) \\ &= constant - 2\,\mathrm{Tr}(f_{\mathbf{\Theta}}(\mathbf{X})\mathbf{L}f_{\mathbf{\Theta}}(\mathbf{X})^\top) \geq 0.\end{aligned} \tag{11}$$

□

Note that Eq. 9 encourages the linear kernel matrix $f_{\mathbf{\Theta}}(\mathbf{X})f_{\mathbf{\Theta}}(\mathbf{X})^\top$ to be close to $\tilde{\mathbf{W}}_w$ while Eq. 10 encourage the linear kernel matrix to be far from the $\tilde{\mathbf{W}}_w$ at the same time.

Our loss follows the non-Euclidean geometry. Below, we demonstrate the relation of Eq. 4 to the Affine-invariant Riemannian metric (AIRM). Indeed, our loss function is bounded from both sides by AIRM and AIRM scaled by $\sqrt{m}$ respectively.

Proposition 5. *Let $\sigma(\mathbf{S})$ be the vector of eigenvalues of $\mathbf{S}$, for any matrix $\mathbf{S}_t, \mathbf{S}_w \in \mathbb{S}^m_{+(+)}$, we have:*

$$\begin{aligned}\|\log((\mathbf{I}+\mathbf{S}_t)^{-1/2}(\mathbf{I}+\mathbf{S}_w)(\mathbf{I}+\mathbf{S}_t)^{-1/2})\|_F &\leq \log\det(\mathbf{I}+\mathbf{S}_t) - \log\det(\mathbf{I}+\mathbf{S}_w) \\ &\leq \sqrt{m}\|\log((\mathbf{I}+\mathbf{S}_t)^{-1/2}(\mathbf{I}+\mathbf{S}_w)(\mathbf{I}+\mathbf{S}_t)^{-1/2})\|_F.\end{aligned} \tag{12}$$

Proof. Given $\mathbf{A} = \mathbf{I} + \mathbf{S}_t$ and $\mathbf{B} = \mathbf{I} + \mathbf{S}_w$, we have:

$$\begin{aligned}\log\det(\mathbf{A}) - \log\det(\mathbf{B}) &= \log(\det(\mathbf{A})\det(\mathbf{B}^{-1})) = \log(\det(\mathbf{A})\det(\mathbf{B}^{-1/2})\det(\mathbf{B}^{-1/2})) \\ &= \mathrm{Tr}\log(\mathbf{B}^{-1/2}\mathbf{A}\mathbf{B}^{-1/2}).\end{aligned} \tag{13}$$

We have $\mathrm{Tr}(\mathbf{A}) = \|\sigma(\mathbf{A})\|_1$, $\|\mathbf{A}\|_F = \|\sigma(\mathbf{A})\|_2$ and $\|\mathbf{x}\|_2 \leq \|\mathbf{x}\|_1 \leq \sqrt{m}\|\mathbf{x}\|_2$. □

Thus, Eq. 4 is an approximation of AIRM between the total scatter matrix and the within-class matrix. Prop. 6 relates the LogDet difference to the regularized Jensen Bregman LogDet Divergence (JBLD).

Definition 1. *Given $\mathbf{A}, \mathbf{B} \in \mathbb{S}^m_{+(+)}$, the regularized Jensen Bregman LogDet Divergence is:*

$$J(\mathbf{A}, \mathbf{B}; \alpha) = \log\det\left(\frac{\mathbf{I}+\alpha\mathbf{A}+\alpha\mathbf{B}}{2}\right) - \frac{1}{2}\big(\log\det(\mathbf{I}+\alpha\mathbf{A}) + \log\det(\mathbf{I}+\alpha\mathbf{B})\big) \ \textit{for} \ \mathbf{A}, \mathbf{B}, \alpha \geq 0, \tag{14}$$

where $\mathbf{I}$ can be interpreted as a regularization to prevent $\det(\mathbf{A}) = 0$ and $\log\det(\mathbf{A}) = -\infty$.

Proposition 6. *For any $\mathbf{S}_w, \mathbf{S}_t \in \mathbb{S}^m_{+(+)}$ and $\alpha \geq 0$, we have:*

$$\begin{aligned}&\delta\Big(\mathbf{S}_t, \mathbf{S}_w; \alpha, \frac{1}{2}\Big) > J(\mathbf{S}_w, \mathbf{S}_b; \alpha) = \\ &\qquad \log\det\left(\frac{\mathbf{I}+\alpha\mathbf{S}_w+\alpha\mathbf{S}_b}{2}\right) - \frac{1}{2}\big(\log\det(\mathbf{I}+\alpha\mathbf{S}_w) + \log\det(\mathbf{I}+\alpha\mathbf{S}_b)\big).\end{aligned} \tag{15}$$

Also, $\delta\Big(\mathbf{S}_t, \mathbf{S}_w; \alpha, \frac{1}{2}\Big) \geq J(\mathbf{S}_w, \mathbf{S}_b; \alpha) - m\log\frac{1}{2}$ where the equality holds if $\log\det(\mathbf{I}+\alpha\mathbf{S}_b) = 0$.

Proof. Based on Eq. 14, we notice JBLD is a lower bound of our loss:

$$\begin{aligned}J(\mathbf{S}_w, \mathbf{S}_b; \alpha) &= \log\det\left(\frac{\mathbf{I}+\alpha\mathbf{S}_w+\alpha\mathbf{S}_b}{2}\right) - \frac{1}{2}\big(\log\det(\mathbf{I}+\alpha\mathbf{S}_w) + \log\det(\mathbf{I}+\alpha\mathbf{S}_b)\big) \\ &= m\log\frac{1}{2} + \log\det(\mathbf{I}+\alpha\mathbf{S}_t) - \frac{1}{2}\big(\log\det(\mathbf{I}+\alpha\mathbf{S}_w) + \log\det(\mathbf{I}+\alpha\mathbf{S}_b)\big) \\ &< \log\det(\mathbf{I}+\alpha\mathbf{S}_t) - \frac{1}{2}\log\det(\mathbf{I}+\alpha\mathbf{S}_w) = \delta\Big(\mathbf{S}_t, \mathbf{S}_w; \alpha, \frac{1}{2}\Big).\end{aligned} \tag{16}$$

□

5.3 Relationship of the LogDet model to the Schatten norm

Below we demonstrate the relationship between the LogDet, Trace and Rank operators, respectively, under the Schatten norm [29] framework. Essential is the following family of objective functions:

$$g_{\alpha,\gamma}(\mathbf{S}) = \frac{1}{c}\sum_{i=1}^{m} \log\left(\alpha\sigma_i(\mathbf{S}) + \gamma\right) = \log\det\left(\alpha\mathbf{S} + \gamma I\right), \quad \alpha, \gamma \geq 0, \tag{17}$$

where $\sigma_i(\mathbf{S}), i = 1, \ldots, m$, are the eigenvalues of either $\mathbf{S}_t \in \mathbb{S}^m_{+(+)}$ or $\mathbf{S}_w \in \mathbb{S}^m_{+(+)}$, which are the total scatter matrix and the within scatter matrix from our experiments, respectively. Moreover, we define a normalization constant c where $c = 1$ or $c = \log(\alpha + \gamma)$ as detailed below.

Given $c = 1$, we have:

$$\lim_{p\to 0} \frac{S^p_{\gamma,p}(\mathbf{S}) - m}{p} = g_{1,\gamma}(\mathbf{S}) \quad \text{where} \quad S_{\gamma,p}(\mathbf{S}) = \left(\sum_{i=1}^{m}\left(\sigma_i(\mathbf{S}) + \gamma\right)^p\right)^{1/p}. \tag{18}$$

From the asymptotic analysis, we conclude that LogDet is an arbitrarily accurate rational approximation of ℓ_0 (the pseudo-norm counting non-zero elements) over the eigenvalues of $\mathbf{S}$.

The case $p = 1$ yields the nuclear norm (trace) which makes the 'smoothed' rank difference of GLEN become equivalent of COLES. The opposing limit case, $p = 0$, recovers the LogDet formula.

One can also recover the exact Rank from the LogDet formulation by:

$$\lim_{\alpha\to\infty} g_{\alpha,1}(\mathbf{S}) = \text{Rank}(\mathbf{S}) \quad \text{if} \quad c = \log(1 + \alpha). \tag{19}$$

This is apparent because:

$$\lim_{\alpha\to\infty} \frac{\log(1 + \alpha\sigma_i)}{\log(1 + \alpha)} = 1 \quad \text{if} \quad \sigma_i > 0 \quad \text{and} \quad \lim_{\alpha\to\infty} \frac{\log(1 + \alpha\sigma_i)}{\log(1 + \alpha)} = 0 \quad \text{if} \quad \sigma_i = 0. \tag{20}$$

6 Experiments

We evaluate GLEN (its LogDet relaxation) on the transductive node classification task and node clustering. GLEN is compared to popular unsupervised, contrastive, and (semi-)supervised approaches. Except for the classifier, unsupervised models do not use labels. To learn similarity/dissimilarity, contrastive models employ the contrastive setting. Labels are used in training the projection layer and classifier in semi-supervised models. A fraction of nodes (*i.e.*, 5 or 20 per class) used in training are labeled in the semi-supervised setting. A SoftMax classifier is used by (semi-)supervised models, while a logistic regression classifier is used by unsupervised and contrastive approaches. See Appendix E for implementation details.

Datasets. GLEN is evaluated on four citation networks: Cora, Citeseer, Pubmed, Cora Full [17, 4] for transductive setting. We also employ the large scale Ogbn-arxiv from OGB [14]. See Appendix D for details of datasets.

Metrics. As fixed data splits [48] often benefit models that overfit, we average results over 50 random splits for each dataset. We evaluate performance for 5 and 20 samples per class. Nonetheless, we also evaluate our model on the standard splits.

Baseline models. We group baseline models into unsupervised, contrastive and (semi-)supervised methods, and implement them in the same framework/testbed. Contrastive methods include DeepWalk [32], GCN+SampledNCE developed as an alternative to GraphSAGE+SampledNCE [10], Graph2Gauss [4], SCE [54], DGI [40], GRACE [63], GCA [64], GraphCL [49] and COLES [62], which are our main competitors. Note that GRACE, GCA and GraphCL are based on multi-view and data augmentation, and GraphCL is mainly intended for graph classification. We do not study graph classification as it requires advanced node pooling with mixed- or high-order statistics [43, 19, 20]. We compare results with representative (semi-)supervised GCN [17], GAT [40] and MixHop [1] models. SGC and S^2GC are unsupervised spectral filter networks. They do not have any learnable parameters. COLES and GLEN can be regarded as dimension reduction techniques for SGC and S^2GC, thus we compare them to PCA-S^2GC and RP-S^2GC, which use PCA and random projections to obtain the projection layer. We set hyperparameters based on the settings described in prior papers.

6.1 Transductive Learning

Below, we consider transductive learning where all nodes are available in the training process.

COLES *vs*. GLEN. Table 1 shows the performance of GLEN *vs*. COLES on two different backbones, *i.e*., GCN and S^2GC. On both backbones, GLEN shows non-trivial improvements on all four datasets. GLEN-S^2GC outperforms COLES by up to 4.6%. Table 2 evaluates GLEN on Cora, Citeseer, PubMed on the standard splits instead of the random splits. See Appendix G for comparisons to additional contrastive learning frameworks.

Contrastive Embedding Baselines *vs*. GLEN. Table 1 shows that GLEN-GCN and GLEN-S^2GC outperform unsupervised models. In particular, GLEN-GCN outperforms GCN+SampledNCE on all four datasets, which shows that GLEN has an advantage over the SampledNCE framework. In addition, GLEN-S^2GC outperforms the best contrastive baseline DGI by up to 3.4%. On Cora with 5 training samples, GLEN-S^2GC outperforms S^2GC by 6.8%. Finally, Table 3 shows that GLEN-S^2GC (small number of trainable parameters) outperforms other methods on the challenging Ogbn-arxiv.

Semi-supervised GNNs *vs*. GLEN. Table 1 shows that the contrastive GCN baselines perform worse than semi-supervised variants, especially when 20 labeled samples per class are available. In contrast, GLEN-GCN outperformed the semi-supervised GCN on Cora by 10% and 3.4% given 5 and 20 labeled samples per class. GLEN-GCN also outperforms GCN on Citeseer and Pubmed by 9.9% and 5.2% given 5 labeled samples per class. These results show the superiority of GLEN on four datasets when the number of samples per class is 5. Even for 20 labeled samples per class, GLEN-S^2GC outperforms the best semi-supervised baselines on all four datasets *e.g*., by 3.3% on Cora. Semi-supervised models (*e.g*., GAT and MixHop) are affected by the low number of labeled samples, which is consistent with [25]. The accuracy of GLEN-GCN and GLEN-S^2GC is unaffected.

Unsupervised GNNs *vs*. GLEN. SGC and S^2GC are unsupervised linear networks based on spectral filters which do not use labels (except for the classifier). GLEN helps both methods reduce the dimension and achieve good discriminative features. Table 1 shows that GLEN-S^2GC outperforms RP-S^2GC and PCA-S^2GC under the same projection size. GLEN-S^2GC also outperforms the unsupervised S^2GC baseline (high-dimensional representation).

6.2 Node Clustering

We compare GLEN-GCN and GLEN-S^2GC with three types of clustering methods:

i. Methods that use only node features, *e.g*., k-means and spectral clustering (spectral-f) construct a similarity matrix with the node features by a linear kernel.

ii. Structural clustering methods that only use the graph structure: spectral clustering (spectral-g) that takes the graph adjacency matrix as the similarity matrix, and DeepWalk [32].

Table 1: Mean classification accuracy (%) and the standard dev. over 50 random splits. Numbers of labeled samples per class are in parentheses. The best accuracy per column is in bold. Models are organized into semi-supervised, contrastive and unsupervised groups. OOM means out of memory.

	Method	Cora		Citeseer		Pubmed		Cora Full	
		(5)	(20)	(5)	(20)	(5)	(20)	(5)	(20)
Semi-supervised	GCN	67.5±4.8	79.4±1.6	57.7±4.7	69.4±1.4	65.4±5.2	77.2±2.1	49.3±1.8	61.5±0.5
	GAT	71.2±3.5	79.6±1.5	54.9±5.0	69.1±1.5	65.5±4.6	75.4±2.3	43.9±1.5	56.9±0.6
	MixHop	67.9±5.7	80.0±1.4	54.5±4.3	67.1±2.0	64.4±5.6	75.7±2.7	47.5±1.5	61.0±0.7
Contrastive	DeepWalk	60.3±4.0	70.5±1.9	38.3±2.9	45.6±2.0	60.3±5.6	70.8±2.6	38.9±1.4	51.1±0.7
	GCN+SampledNCE	61.3±4.3	74.3±1.6	42.3±3.4	56.8±1.9	60.9±5.7	70.3±2.5	32.7±1.9	45.2±0.9
	SAGE+SampledNCE	65.0±3.5	73.8±1.5	48.0±3.5	56.5±1.6	64.1±6.1	74.6±1.9	35.0±1.4	43.6±0.6
	Graph2Gauss	72.7±2.0	76.2±1.1	60.7±3.5	65.7±1.5	67.6±3.9	74.1±2.1	38.9±1.3	49.3±0.5
	SCE	74.3±2.7	80.2±1.1	65.4±2.9	70.7±1.2	65.7±6.0	75.8±2.2	50.7±1.5	60.6±0.6
	DGI	72.9±4.0	78.1±1.8	65.7±3.6	71.1±1.1	65.3±5.7	73.9±2.3	50.5±1.4	58.4±0.6
	COLES-GCN	73.8±3.4	80.8±1.3	66.0±2.6	69.0±1.3	62.7±4.6	72.7±2.1	47.3±1.5	58.9±0.5
	COLES-GCN (Stiefel)	75.0±3.4	81.0±1.3	67.9±2.3	71.7±0.9	62.6±5.0	73.2±2.6	47.6±1.2	59.2±0.5
	COLES-S^2GC	76.5±2.6	81.5±1.2	67.5±2.2	71.3±1.0	66.0±5.2	77.4±1.9	51.2±1.4	61.8±0.5
	GLEN-GCN	77.5±2.6	82.7±1.2	67.6±2.6	72.0±0.9	68.7±5.7	78.2±2.4	52.7±1.5	62.0±0.5
	GLEN-S^2GC	**78.2±2.4**	**83.0±1.0**	**69.1±2.1**	**72.3±0.9**	**70.6±3.9**	**80.1±1.9**	**53.0±1.5**	**62.6±0.5**
Contrastive + Multiview	GraphCL	72.6±4.2	78.3±1.7	65.6±3.0	71.1±0.8	OOM	OOM	OOM	OOM
	GRACE	64.9±4.2	73.9±1.6	61.8±3.9	68.4±1.6	OOM	OOM	OOM	OOM
	GCA	61.5±4.9	75.8±1.9	43.2±3.6	55.7±1.9	OOM	OOM	OOM	OOM
Unsupervised	SGC	63.9±5.4	78.3±1.9	59.5±3.4	69.8±1.4	65.8±4.4	76.3±2.3	46.0±2.2	57.7±1.2
	S^2GC	71.4±4.4	81.3±1.2	60.3±4.0	69.5±1.2	67.6±4.2	73.3±2.0	41.8±1.7	60.0±0.5
	PCA-S^2GC	72.1±3.8	81.2±1.3	61.0±3.5	68.8±1.3	67.5±4.3	73.2±2.0	42.3±1.7	59.3±0.6
	RP-S^2GC	65.9±4.6	78.1±1.2	51.4±3.2	61.7±1.6	66.1±5.0	72.5±1.9	31.5±1.4	48.7±0.6

iii. Attributed graph clustering methods that use node features and the graph: Graph Autoencoder (GAE), Graph Variational Autoencoder (VGAE) [17], Adversarially Regularized Graph Autoencoder (ARGE), Var. Graph Autoencoder (ARVGE) [31], SGC [45] , S^2GC [60], COLES [62].

We measure and report the clustering Accuracy (Acc), Normalized Mutual Information (NMI) and macro F1-score (F1). We run each method 10 times on Cora, CiteSeer and PubMed. We follow [55] and set the number of propagation steps to 8 for SGC, S^2GC, COLES-S^2GC and COLES-S^2GC. Table 4 shows that GLEN-S^2GC outperforms other methods in all cases, whereas GLEN-GCN outperforms COLES-GCN, COLES-GCN (Stiefel) and contrastive GCN on all datasets.

6.3 Comparison of Surrogates of Rank

Table 5 shows results on four additional surrogates of Rank($\mathbf{S}$):

- Nuclear norm: $R_{\text{NN}}(\mathbf{S}) = \sum_i \sigma_i(\mathbf{S})$.
- γ-nuclear norm [16]: $R_{\gamma\text{-NN}} = \sum_i \frac{(1+\gamma)\sigma_i(\mathbf{S})}{\gamma+\sigma_i(\mathbf{S})}$.
- S_p norm [29]: $R_{S_p} = \sum_i \sigma_i(\mathbf{S})^p$.
- Geman norm [8]: $R_{\text{Geman}} = \sum_i \frac{\sigma_i(\mathbf{S})}{\gamma+\sigma_i(\mathbf{S})}$.

6.4 Transductive One-shot Learning for Image Recognition

The most common setting in few-shot learning [35, 37, 50, 26, 53, 51, 52] is the inductive setting. In such a scenario, only samples in the support set can be used to fine-tune the model or learn a function for the inference of query labels. In contrast, in the transductive scenario, the model has access to all the query data (unlabeled) that needs to be classified.

EASE [61] is a transductive few-shot learner for so-called episodic image classification. Given feature matrix $\mathbf{Z} \in \mathbb{R}^{n\times m}$ from a CNN backbone (ResNet-12), EASE minimizes $\text{Tr}(\mathbf{U}\mathbf{Z}^\top\mathbf{L}_w\mathbf{Z}\mathbf{U}^\top) - \text{Tr}(\mathbf{U}\mathbf{Z}^\top\mathbf{L}_t\mathbf{Z}\mathbf{U}^\top)$ (subject to $\mathbf{U}\mathbf{U}^\top = \mathbf{I}$) in order to learn a linear projection $\mathbf{U}$.

We extend EASE with the objective of GLEN to learn the linear projection $\mathbf{U}$ by minimizing $\log\det(\mathbf{U}\mathbf{Z}^\top\mathbf{L}_w\mathbf{Z}\mathbf{U}^\top) - \log\det(\mathbf{U}\mathbf{Z}^\top\mathbf{L}_t\mathbf{Z}\mathbf{U}^\top)$ (subject to $\mathbf{U}\mathbf{U}^\top = \mathbf{I}$. We also apply the S_p norm instead of LogDet. Table 6 shows the results of EASE with the LogDet-based relaxation and the S_p-norm based relaxation of GLEN. For the simplicity of the experiment, we use soft k-means rather than Sinkhorn k-means as in the original EASE pipeline. See EASE [61] for the experimental setting.

We evaluate our approach on four few-shot classification benchmarks, mini-ImageNet [41], tiered-ImageNet [33], CUB [44], and CIFAR-FS [21]. The performance numbers are given as accuracy (%) and the 0.95 confidence intervals are reported. We use publicly available pre-trained ResNet-12 [30] that is trained on the base-class training split.

Table 2: Comparison with other methods on Cora, Citeseer and PubMed on standard splits.

	Cora	Citeseer	Pubmed
GCN	81.5	70.3	79.0
GAT	83.0	72.5	79.0
DeepWalk+F	77.36	64.30	69.65
Node2vec+F	75.44	63.22	70.60
GAE	73.68	58.21	76.16
VGAE	77.44	59.53	78.00
DGI	81.26	69.50	77.70
GRACE	81.9	71.2	80.6
GraphCL	81.89	68.40	OOM
GMI	80.28	65.99	OOM
COLES-GNN	81.9	70.3	79.1
GLEN-S^2GC	**85.10**	**71.90**	**80.72**

Table 3: Mean classification accuracy (%) and the standard dev. over 10 runs on Ogbn-arxiv. Results of other models are from original papers.

Method		Test Acc.	#Params
MLP		55.50±0.23	110,120
Node2Vec	[9]	70.07±0.13	21,818,792
GraphZoom	[6]	71.18±0.18	8,963,624
C&S	[15]	71.26±0.01	5,160
SAGE-mean	[10]	71.49±0.27	218,664
GCN	[17]	71.74±0.29	142,888
DeeperGCN	[24]	71.92±0.17	491,176
SIGN	[34]	71.95±0.11	3,566,128
FrameLet	[58]	71.97±0.12	1,633,183
S^2GC	[60]	72.01±0.25	110,120
COLES-S^2GC	[62]	72.48±0.25	110,120
GLEN-S^2GC		**72.67±0.26**	110,120

Table 4: The clustering performance on Cora, Citeseer and Pubmed.

Method	Input	Cora			Citeseer			Pubmed		
		Acc%	NMI%	F1%	Acc%	NMI%	F1%	Acc%	NMI%	F1%
k-means	Feature	34.65	16.73	25.42	38.49	17.02	30.47	57.32	29.12	57.35
Spectral-f	Feature	36.26	15.09	25.64	46.23	21.19	33.70	59.91	32.55	58.61
Spectral-g	Graph	34.19	19.49	30.17	25.91	11.84	29.48	39.74	3.46	51.97
DeepWalk	Graph	46.74	31.75	38.06	36.15	9.66	26.70	61.86	16.71	47.06
GAE	Both	53.25	40.69	41.97	41.26	18.34	29.13	64.08	22.97	49.26
VGAE	Both	55.95	38.45	41.50	44.38	22.71	31.88	65.48	25.09	50.95
ARGE	Both	64.00	44.90	61.90	57.30	35.00	54.60	59.12	23.17	58.41
ARVGE	Both	62.66	45.28	62.15	54.40	26.10	52.90	58.22	20.62	23.04
GCN	Both	59.05	43.06	59.38	45.97	20.08	45.57	61.88	25.48	60.70
SGC	Both	62.87	50.05	58.60	52.77	32.90	63.90	69.09	31.64	68.45
S^2GC	Both	68.96	54.22	65.43	69.11	42.87	64.65	68.18	31.82	67.81
COLES-GCN	Both	60.74	45.49	59.33	63.28	37.54	59.17	63.46	25.73	63.42
COLES-GCN (Stiefel)	Both	62.46	47.01	59.38	65.17	38.90	60.85	63.56	25.81	63.58
COLES-S^2GC	Both	69.70	55.35	63.06	69.20	44.41	64.70	68.76	33.42	68.12
GLEN-GCN	Both	69.27	55.34	62.14	68.25	42.98	64.10	64.64	30.08	64.12
GLEN-S^2GC	Both	**71.01**	**56.69**	**69.01**	**69.89**	**45.37**	**65.70**	**69.62**	**34.97**	**69.33**

Table 5: Mean classification accuracy (%) and the standard dev. over 50 random splits. Numbers of labeled samples per class are in parentheses. The best accuracy per column is in bold. Models are organized into semi-supervised, contrastive and unsupervised groups. OOM means out of memory.

Method	Cora		Citeseer		Pubmed		Cora Full	
	(5)	(20)	(5)	(20)	(5)	(20)	(5)	(20)
GLEN (Nuclear Norm)	76.5±2.6	81.5±1.2	67.5±2.2	71.3±1.0	66.0±5.2	77.4±1.9	50.8±1.4	61.8±0.5
GLEN (γ-nuclear norm)	71.8±3.0	77.6±1.3	63.2±3.1	69.3±0.8	71.2±4.3	78.1±1.5	49.2±1.4	60.6±0.6
GLEN (S_p norm)	75.2±3.5	80.7±1.2	64.7±2.4	70.9.±0.9	65.9±5.5	73.9±2.4	48.0±1.6	59.7±1.6
GLEN (Geman norm)	72.3±2.5	77.2±1.3	65.4±2.2	70.7.±0.8	**72.6±4.5**	78.3±1.5	49.2±1.5	60.6±1.6
GLEN (LogDet)	**78.2±2.4**	**83.0±1.0**	**69.1±2.1**	**72.3±0.9**	70.6±3.9	**80.1±1.9**	**53.0±1.5**	**62.6±0.5**

Table 6: One-shot learning in the transductive setting on EASE based on GLEN.

methods	*mini*–Imagenet [41]	*tiered*–Imagenet [33]	CIFAR–FS [21]	CUB [44]
EASE [61]	58.2±0.19	70.9±0.21	65.2±0.21	77.7±0.19
EASE GLEN (S_p norm)	60.5±0.23	74.8±0.25	67.8±0.25	81.5±0.25
EASE GLEN (LogDet)	**61.4±0.23**	**76.4±0.25**	**69.2±0.25**	**83.4±0.25**

Scalability. GraphSAGE and DGI require neighbor sampling with redundant forward/backward steps (long runtime). In contrast, GLEN-S^2GC enjoys a simple implementation with low memory usage/low runtime. For graphs with over thousands of nodes and millions edges (OGB benchmark), GLEN runs fast on NVIDIA 1080 GPU. Even on larger graph benchmarks, GLEN is fast as it optimizes the total scatter and the within-class matrices whose size depends on the embedding size rather than the node number. The runtime of GLEN-S^2GC is also favourable in comparison to multi-view augmentation-based GraphCL. Specifically, GLEN-S^2GC took 0.54s, 0.3s, 5.3s and 15.4s on Cora, Citeseer, Pubmed and Cora Full, respectively. GraphCL took 110.19s, 101.0s, $\geq$ 8h and $\geq$ 8h respectively. Although the LogDet difference is somewhat slower than the trace difference in forward/backward propagation, it converges faster, thus enjoying a similar low runtime.

7 Conclusions

In this paper, we model contrastvie learning as a rank difference problem to approximate the condition that the rank of total scatter matrix should equal the sum of ranks of within-scatter and between-scatter matrices. We relax this NP-hard problem with a differentiable difference of LogDet terms. We also show two perspectives on GLEN and the existing methods based on the low-rank optimization and distance between symmetric positive (semi-)definite matrices. In low-rank optimization, we explain why the LogDet difference is a better surrogate to optimize rank difference compared to the trace difference. We also show that our solution encourages linear kernel of embeddings become the geometric mean between the total scatter matrix and the within-class scatter matrix. GLEN works well with many backbones and outperforms many unsupervised, contrastive and (semi-)supervised methods.

Acknowledgments and Disclosure of Funding

We thank reviewers for stimulating questions that helped us improve several aspects of our analysis. Hao Zhu is supported by an Australian Government Research Training Program (RTP) Scholarship. Piotr Koniusz is supported by CSIRO's Machine Learning and Artificial Intelligence Future Science Platform (MLAI FSP).

References

[1] Sami Abu-El-Haija, Bryan Perozzi, Amol Kapoor, Nazanin Alipourfard, Kristina Lerman, Hrayr Harutyunyan, Greg Ver Steeg, and Aram Galstyan. Mixhop: Higher-order graph convolutional architectures via sparsified neighborhood mixing. In *International Conference on Machine Learning*, pages 21–29, 2019.

[2] Philip Bachman, R Devon Hjelm, and William Buchwalter. Learning representations by maximizing mutual information across views. *arXiv preprint arXiv:1906.00910*, 2019.

[3] Mikhail Belkin and Partha Niyogi. Laplacian eigenmaps for dimensionality reduction and data representation. *Neural computation*, 15(6):1373–1396, 2003.

[4] Aleksandar Bojchevski and Stephan Günnemann. Deep gaussian embedding of graphs: Unsupervised inductive learning via ranking. *arXiv preprint arXiv:1707.03815*, 2017.

[5] Hongyun Cai, Vincent W Zheng, and Kevin Chen-Chuan Chang. A comprehensive survey of graph embedding: Problems, techniques, and applications. *IEEE Transactions on Knowledge and Data Engineering*, 30(9):1616–1637, 2018.

[6] C Deng, Z Zhao, Y Wang, Z Zhang, and Z Feng. Graphzoom: A multi-level spectral approach for accurate and scalable graph embedding. In *International Conference on Learning Representations*, 2020.

[7] Maryam Fazel, Haitham Hindi, and Stephen P Boyd. Log-det heuristic for matrix rank minimization with applications to hankel and euclidean distance matrices. In *Proceedings of the 2003 American Control Conference, 2003.*, volume 3, pages 2156–2162. IEEE, 2003.

[8] Donald Geman and Chengda Yang. Nonlinear image recovery with half-quadratic regularization. *IEEE transactions on Image Processing*, 4(7):932–946, 1995.

[9] Aditya Grover and Jure Leskovec. node2vec: Scalable feature learning for networks. In *ACM SIGKDD international conference on Knowledge discovery and Data Mining*, pages 855–864, 2016.

[10] Will Hamilton, Zhitao Ying, and Jure Leskovec. Inductive representation learning on large graphs. In *Advances in Neural Information Processing Systems*, pages 1024–1034, 2017.

[11] Kaveh Hassani and Amir Hosein Khasahmadi. Contrastive multi-view representation learning on graphs. In *International Conference on Machine Learning*, pages 4116–4126, 2020.

[12] Xiaofei He and Partha Niyogi. Locality preserving projections. *Advances in Neural Information Processing Systems*, 16(16):153–160, 2004.

[13] R Devon Hjelm, Alex Fedorov, Samuel Lavoie-Marchildon, Karan Grewal, Phil Bachman, Adam Trischler, and Yoshua Bengio. Learning deep representations by mutual information estimation and maximization. *arXiv preprint arXiv:1808.06670*, 2018.

[14] Weihua Hu, Matthias Fey, Marinka Zitnik, Yuxiao Dong, Hongyu Ren, Bowen Liu, Michele Catasta, and Jure Leskovec. Open graph benchmark: Datasets for machine learning on graphs. *arXiv preprint arXiv:2005.00687*, 2020.

[15] Qian Huang, Horace He, Abhay Singh, Ser-Nam Lim, and Austin Benson. Combining label propagation and simple models out-performs graph neural networks. In *International Conference on Learning Representations*, 2021.

[16] Zhao Kang, Chong Peng, and Qiang Cheng. Robust pca via nonconvex rank approximation. In *2015 IEEE International Conference on Data Mining*, pages 211–220. IEEE, 2015.

[17] Thomas N Kipf and Max Welling. Semi-supervised classification with graph convolutional networks. *arXiv preprint arXiv:1609.02907*, 2016.

[18] Thomas N Kipf and Max Welling. Variational graph auto-encoders. *arXiv preprint arXiv:1611.07308*, 2016.

[19] Piotr Koniusz, Lei Wang, and Anoop Cherian. Tensor representations for action recognition. *IEEE Trans. Pattern Anal. Mach. Intell.*, 44(2):648–665, 2022.

[20] Piotr Koniusz and Hongguang Zhang. Power normalizations in fine-grained image, few-shot image and graph classification. *IEEE Trans. Pattern Anal. Mach. Intell.*, 44(2):591–609, 2022.

[21] Alex Krizhevsky, Geoffrey Hinton, et al. Learning multiple layers of features from tiny images. 2009.

[22] Brian Kulis et al. Metric learning: A survey. *Foundations and Trends® in Machine Learning*, 5(4):287–364, 2013.

[23] Omer Levy and Yoav Goldberg. Neural word embedding as implicit matrix factorization. *Advances in Neural Information Processing Systems*, 27:2177–2185, 2014.

[24] Guohao Li, Chenxin Xiong, Ali Thabet, and Bernard Ghanem. Deepergcn: All you need to train deeper gcns. *arXiv preprint arXiv:2006.07739*, 2020.

[25] Qimai Li, Zhichao Han, and Xiao-Ming Wu. Deeper insights into graph convolutional networks for semi-supervised learning. In *AAAI Conference on Artificial Intelligence*, pages 3538–3545, 2018.

[26] Changsheng Lu and Piotr Koniusz. Few-shot keypoint detection with uncertainty learning for unseen species. *IEEE Conference on Computer Vision and Pattern Recognition*, 2022.

[27] Tomas Mikolov, Kai Chen, Greg Corrado, and Jeffrey Dean. Efficient estimation of word representations in vector space. *arXiv preprint arXiv:1301.3781*, 2013.

[28] Tomas Mikolov, Ilya Sutskever, Kai Chen, Gregory S Corrado, and Jeffrey Dean. Distributed representations of words and phrases and their compositionality. In *Advances in Neural Information Processing Systems*, 2013.

[29] Karthik Mohan and Maryam Fazel. Iterative reweighted algorithms for matrix rank minimization. *The Journal of Machine Learning Research*, 13(1):3441–3473, 2012.

[30] Boris N Oreshkin, Pau Rodriguez, and Alexandre Lacoste. Tadam: Task dependent adaptive metric for improved few-shot learning. *arXiv preprint arXiv:1805.10123*, 2018.

[31] S Pan, R Hu, G Long, J Jiang, L Yao, and C Zhang. Adversarially regularized graph autoencoder for graph embedding. In *International Joint Conference on Artificial Intelligence*, 2018.

[32] Bryan Perozzi, Rami Al-Rfou, and Steven Skiena. Deepwalk: Online learning of social representations. In *ACM SIGKDD International Conference on Knowledge Discovery and Data Mining*, pages 701–710, 2014.

[33] Mengye Ren, Eleni Triantafillou, Sachin Ravi, Jake Snell, Kevin Swersky, Joshua B Tenenbaum, Hugo Larochelle, and Richard S Zemel. Meta-learning for semi-supervised few-shot classification. *arXiv preprint arXiv:1803.00676*, 2018.

[34] Emanuele Rossi, Fabrizio Frasca, Ben Chamberlain, Davide Eynard, Michael Bronstein, and Federico Monti. Sign: Scalable inception graph neural networks. *arXiv preprint arXiv:2004.11198*, 2020.

[35] Jake Snell, Kevin Swersky, and Richard Zemel. Prototypical networks for few-shot learning. In *Advances in Neural Information Processing Systems*, pages 4077–4087, 2017.

[36] Ke Sun, Piotr Koniusz, and Zhen Wang. Fisher-bures adversary graph convolutional networks. *Conference on Uncertainty in Artificial Intelligence*, 115:465–475, 2019.

[37] Flood Sung, Yongxin Yang, Li Zhang, Tao Xiang, Philip HS Torr, and Timothy M Hospedales. Learning to compare: Relation network for few-shot learning. *arXiv preprint arXiv:1711.06025*, 2017.

[38] Jian Tang, Meng Qu, Mingzhe Wang, Ming Zhang, Jun Yan, and Qiaozhu Mei. Line: Large-scale information network embedding. In *International Conference on World Wide Web*, pages 1067–1077, 2015.

[39] Joshua B Tenenbaum, Vin De Silva, and John C Langford. A global geometric framework for nonlinear dimensionality reduction. *Science*, 290(5500):2319–2323, 2000.

[40] Petar Velickovic, William Fedus, William L Hamilton, Pietro Lio, Yoshua Bengio, and R Devon Hjelm. Deep graph infomax. In *International Conference on Learning Representations*, 2019.

[41] Oriol Vinyals, Charles Blundell, Timothy Lillicrap, Koray Kavukcuoglu, and Daan Wierstra. Matching networks for one shot learning. *arXiv preprint arXiv:1606.04080*, 2016.

[42] Tongzhou Wang and Phillip Isola. Understanding contrastive representation learning through alignment and uniformity on the hypersphere. In *International Conference on Machine Learning*, volume 119, pages 9929–9939, 2020.

[43] Zhengyang Wang and Shuiwang Ji. Second-order pooling for graph neural networks. *IEEE Transactions on Pattern Analysis and Machine Intelligence*, 2020.

[44] Peter Welinder, Steve Branson, Takeshi Mita, Catherine Wah, Florian Schroff, Serge Belongie, and Pietro Perona. Caltech-ucsd birds 200. 2010.

[45] Felix Wu, Tianyi Zhang, Amauri Holanda de Souza Jr, Christopher Fifty, Tao Yu, and Kilian Q Weinberger. Simplifying graph convolutional networks. *arXiv preprint arXiv:1902.07153*, 2019.

[46] Shuicheng Yan, Dong Xu, Benyu Zhang, Hong-jiang Zhang, Qiang Yang, and Stephen Lin. Graph embedding and extensions: A general framework for dimensionality reduction. *IEEE Transactions on Pattern Analysis and Machine Intelligence*, 29(1):40–51, 2007.

[47] Zhen Yang, Ming Ding, Chang Zhou, Hongxia Yang, Jingren Zhou, and Jie Tang. Understanding negative sampling in graph representation learning. In *ACM SIGKDD International Conference on Knowledge Discovery and Data Mining*, pages 1666–1676, 2020.

[48] Zhilin Yang, William Cohen, and Ruslan Salakhudinov. Revisiting semi-supervised learning with graph embeddings. In *International Conference on Machine Learning*, pages 40–48, 2016.

[49] Yuning You, Tianlong Chen, Yongduo Sui, Ting Chen, Zhangyang Wang, and Yang Shen. Graph contrastive learning with augmentations. *Advances in Neural Information Processing Systems*, 33:5812–5823, 2020.

[50] Chi Zhang, Yujun Cai, Guosheng Lin, and Chunhua Shen. Deepemd: Few-shot image classification with differentiable earth mover's distance and structured classifiers. *IEEE Conference on Computer Vision and Pattern Recognition*, pages 12203–12213, 2020.

[51] Hongguang Zhang, Hongdong Li, and Piotr Koniusz. Multi-level second-order few-shot learning. *IEEE Transactions on Multimedia*, 2022.

[52] Shan Zhang, Naila Murray, Lei Wang, and Piotr Koniusz. Time-rEversed diffusioN tEnsor Transformer: A new TENET of Few-Shot Object Detection. *European Conference on Computer Vision*, 2022.

[53] Shan Zhang, Lei Wang, Naila Murray, and Piotr Koniusz. Kernelized few-shot object detection with efficient integral aggregation. *IEEE Conference on Computer Vision and Pattern Recognition*, pages 19207–19216, 2022.

[54] Shengzhong Zhang, Zengfeng Huang, Haicang Zhou, and Ziang Zhou. Sce: Scalable network embedding from sparsest cut. In *ACM SIGKDD International Conference on Knowledge Discovery and Data Mining*, pages 257–265, 2020.

[55] Xiaotong Zhang, Han Liu, Qimai Li, and Xiao-Ming Wu. Attributed graph clustering via adaptive graph convolution. *arXiv preprint arXiv:1906.01210*, 2019.

[56] Yifei Zhang, Hao Zhu, Ziqiao Meng, Piotr Koniusz, and Irwin King. Graph-adaptive rectified linear unit for graph neural networks. In *Proceedings of the Web Conference*, pages 1331–1339. ACM, 2022.

[57] Yifei Zhang, Hao Zhu, Zixing Song, Piotr Koniusz, and Irwin King. COSTA: covariance-preserving feature augmentation for graph contrastive learning. In *ACM SIGKDD International Conference on Knowledge Discovery and Data Mining*, pages 2524–2534. ACM, 2022.

[58] Xuebin Zheng, Bingxin Zhou, Junbin Gao, Yuguang Wang, Pietro Lió, Ming Li, and Guido Montufar. How framelets enhance graph neural networks. In Marina Meila and Tong Zhang, editors, *International Conference on Machine Learning*, volume 139, pages 12761–12771, 2021.

[59] Hao Zhu and Piotr Koniusz. REFINE: Random range finder for network embedding. In *ACM Conference on Information and Knowledge Management*, 2021.

[60] Hao Zhu and Piotr Koniusz. Simple spectral graph convolution. In *International Conference on Learning Representations*, 2021.

[61] Hao Zhu and Piotr Koniusz. EASE: Unsupervised discriminant subspace learning for transductive few-shot learning. In *Proceedings of the IEEE/CVF Conference on Computer Vision and Pattern Recognition*, pages 9078–9088, 2022.

[62] Hao Zhu, Ke Sun, and Piotr Koniusz. Contrastive laplacian eigenmaps. *Advances in Neural Information Processing Systems*, 34, 2021.

[63] Yanqiao Zhu, Yichen Xu, Feng Yu, Qiang Liu, Shu Wu, and Liang Wang. Deep graph contrastive representation learning. *arXiv preprint arXiv:2006.04131*, 2020.

[64] Yanqiao Zhu, Yichen Xu, Feng Yu, Qiang Liu, Shu Wu, and Liang Wang. Graph contrastive learning with adaptive augmentation. In *Proceedings of the Web Conference*, pages 2069–2080, 2021.

Checklist

The checklist follows the references. Please read the checklist guidelines carefully for information on how to answer these questions. For each question, change the default **[TODO]** to [Yes] , [No] , or [N/A] . You are strongly encouraged to include a **justification to your answer**, either by referencing the appropriate section of your paper or providing a brief inline description. For example:

- Did you include the license to the code and datasets? [Yes] See Section ?.
- Did you include the license to the code and datasets? [No] The code and the data are proprietary.
- Did you include the license to the code and datasets? [N/A]

Please do not modify the questions and only use the provided macros for your answers. Note that the Checklist section does not count towards the page limit. In your paper, please delete this instructions block and only keep the Checklist section heading above along with the questions/answers below.

i. For all authors...
   (a) Do the main claims made in the abstract and introduction accurately reflect the paper's contributions and scope? [Yes]
   (b) Did you describe the limitations of your work? [Yes]
   (c) Did you discuss any potential negative societal impacts of your work? [N/A]
   (d) Have you read the ethics review guidelines and ensured that your paper conforms to them? [Yes]

ii. If you are including theoretical results...
   (a) Did you state the full set of assumptions of all theoretical results? [Yes]
   (b) Did you include complete proofs of all theoretical results? [Yes]

iii. If you ran experiments...
   (a) Did you include the code, data, and instructions needed to reproduce the main experimental results (either in the supplemental material or as a URL)? [N/A]
   (b) Did you specify all the training details (*e.g.*, data splits, hyperparameters, how they were chosen)? [Yes]
   (c) Did you report error bars (*e.g.*, with respect to the random seed after running experiments multiple times)? [Yes]
   (d) Did you include the total amount of compute and the type of resources used (*e.g.*, type of GPUs, internal cluster, or cloud provider)? [Yes]

iv. If you are using existing assets (*e.g.*, code, data, models) or curating/releasing new assets...
   (a) If your work uses existing assets, did you cite the creators? [Yes]
   (b) Did you mention the license of the assets? [Yes]
   (c) Did you include any new assets either in the supplemental material or as a URL? [No]
   (d) Did you discuss whether and how consent was obtained from people whose data you're using/curating? [N/A]
   (e) Did you discuss whether the data you are using/curating contains personally identifiable information or offensive content? [N/A]

v. If you used crowdsourcing or conducted research with human subjects...
   (a) Did you include the full text of instructions given to participants and screenshots, if applicable? [N/A]
   (b) Did you describe any potential participant risks, with links to Institutional Review Board (IRB) approvals, if applicable? [N/A]
   (c) Did you include the estimated hourly wage paid to participants and the total amount spent on participant compensation? [N/A]

Generalized Laplacian Eigenmaps (Supplementary Material)

Hao Zhu[†,§] **Piotr Koniusz**[*,§,†]
[§]Data61/CSIRO [†]Australian National University
allenhaozhu@gmail.com, piotr.koniusz@data61.csiro.au

A Spectrum Analysis

Below we analyze the spectrum of embedding matrix $f_{\boldsymbol{\Theta}}(\mathbf{X})$ for several different objectives to show that GLEN enjoys better embedding properties than COLES [72].

Without decorrelation term $\|f_{\boldsymbol{\Theta}}(\mathbf{X})^\top f_{\boldsymbol{\Theta}}(\mathbf{X}) - \mathbf{I}\|_F^2$ used by COLES, the trace-based objective in Eq. 6 optimization may results in the so-called dimensional collapse which means that the vast majority of singular values of embeddings are zeroed and only one or two leading components are non-zero.

Fig. 2b shows that in COLES the sixth singular value and the following singular values are almost equal zero, whereas the first singular value is over 2600 in value, thus dominating the spectrum. Fig. 2a shows that our GLEN based on the LogDet difference of terms performs better than COLES. Firstly, the first leading singular value is not as large as COLES (only 80) so it does not dominate the spectrum. The next singular values follow a gradual decline. It is worth noting that even with the decorrelation term $\|f_{\boldsymbol{\Theta}}(\mathbf{X})^\top f_{\boldsymbol{\Theta}}(\mathbf{X}) - \mathbf{I}\|_F^2$ used by COLES, it only helps the first five leading singular values, and the first singular value is still larger than the counterpart of GLEN (393 *vs*. 80).

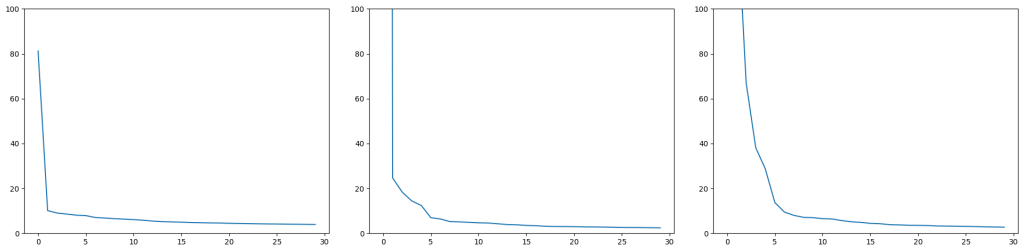

(a) GLEN (b) COLES (c) with decorrelation

Figure 2: Singular values of embeddings showing the values of the first 30 leading singular values. For comparison purposes, we truncate the range of singular values for COLES. The first singular value of COLES is 2650 (very large value). The range of singular values with the use of decorrelation term is 393. The decorrelation term penalizes $\|f_{\boldsymbol{\Theta}}(\mathbf{X})^\top f_{\boldsymbol{\Theta}}(\mathbf{X}) - \mathbf{I}\|_F^2$. Notice that the spectrum of GLEN is more balanced.

B Nuclear Norm *vs*. LogDet for Rank Minimization

In our paper, to facilitate the analysis we assume $\mathrm{Rank}(\mathbf{S}) \leq \log\det(\mathbf{I}+\mathbf{S}) \leq \mathrm{Tr}(\mathbf{S})$. Below we clarify the necessary conditions for this inequality to hold true.

Proposition 7. *Let* $\mathbf{S} \in \mathbb{S}_{+(+)}^m$, *if* $\mathrm{Tr}(\mathbf{S}) \geq m$ *then* $\mathrm{Rank}(\mathbf{S}) \leq \log\det(\mathbf{I}+\mathbf{S}) \leq \mathrm{Tr}(\mathbf{S})$.

[*]The corresponding author. Code: `https://github.com/allenhaozhu/GLEN`.

36th Conference on Neural Information Processing Systems (NeurIPS 2022).

Proof. It is easy to observe that $\mathrm{Rank}(\mathbf{S}) \leq \mathrm{Tr}(\mathbf{S})$ if $\mathrm{Tr}(\mathbf{S}) \geq m$. Moreover, we have $\mathrm{Tr}(\mathbf{S}) > \mathrm{Tr}(\log(\mathbf{I}+\mathbf{S})) = \log\det(\mathbf{I}+\mathbf{S})$. Let $\mathrm{Rank}(\mathbf{S}) = n \leq m \leq \mathrm{Tr}(\mathbf{S})$, then we have $\log(1+\mathrm{Tr}(\mathbf{S})) \leq \sum_i^m \log(1+\sigma_i(\mathbf{S})) \leq \sum_i^m \log(\mathbf{I}+\mathrm{Tr}(\mathbf{S})/m)$ and $\sum_i^m \log(1+\mathrm{Tr}(\mathbf{S})/m) \geq \sum_i^n \log(1+m/n) \geq \sum_i^m \log(1+m/m) \geq \mathrm{Rank}(\mathbf{S})$. □

C Gradient Analysis

Proposition 8. *The objective of optimization, $f_{\boldsymbol{\Theta}}(\mathbf{X})^\top \mathbf{L}_t = f_{\boldsymbol{\Theta}}(\mathbf{X})^\top \mathbf{L}_w$, is achieved when the following gradient rule is zeroed.*

Proof.

$$\begin{aligned}
\frac{\partial \log\det\left(\mathbf{I}+\alpha f_{\boldsymbol{\Theta}}(\mathbf{X})^\top \mathbf{L}_t f_{\boldsymbol{\Theta}}(\mathbf{X})\right)}{\partial f_{\boldsymbol{\Theta}}(\mathbf{X})} &= \alpha\left(\mathbf{I}+\alpha f_{\boldsymbol{\Theta}}(\mathbf{X})^\top \mathbf{L}_t f_{\boldsymbol{\Theta}}(\mathbf{X})\right)^{-1} f_{\boldsymbol{\Theta}}(\mathbf{X})^\top \mathbf{L}_t, \\
\frac{\partial \log\det\left(\mathbf{I}+\alpha f_{\boldsymbol{\Theta}}(\mathbf{X})^\top \mathbf{L}_w f_{\boldsymbol{\Theta}}(\mathbf{X})\right)}{\partial f_{\boldsymbol{\Theta}}(\mathbf{X})} &= \alpha\left(\mathbf{I}+\alpha f_{\boldsymbol{\Theta}}(\mathbf{X})^\top \mathbf{L}_w f_{\boldsymbol{\Theta}}(\mathbf{X})\right)^{-1} f_{\boldsymbol{\Theta}}(\mathbf{X})^\top \mathbf{L}_w,
\end{aligned} \tag{21}$$

$$\begin{aligned}
&\frac{\partial \log\det\left(\mathbf{I}+\alpha f_{\boldsymbol{\Theta}}(\mathbf{X})^\top \mathbf{L}_t f_{\boldsymbol{\Theta}}(\mathbf{X})\right)}{\partial \mathbf{Z}} - \frac{\partial \log\det\left(\mathbf{I}+\alpha f_{\boldsymbol{\Theta}}(\mathbf{X})^\top \mathbf{L}_w f_{\boldsymbol{\Theta}}(\mathbf{X})\right)}{\partial \mathbf{Z}} = 0 \Leftrightarrow \\
&\left(\mathbf{I}+\alpha f_{\boldsymbol{\Theta}}(\mathbf{X})^\top \mathbf{L}_t f_{\boldsymbol{\Theta}}(\mathbf{X})\right)^{-1} f_{\boldsymbol{\Theta}}(\mathbf{X})^\top \mathbf{L}_t - \left(\mathbf{I}+\alpha f_{\boldsymbol{\Theta}}(\mathbf{X})^\top \mathbf{L}_w f_{\boldsymbol{\Theta}}(\mathbf{X})\right)^{-1} f_{\boldsymbol{\Theta}}(\mathbf{X})^\top \mathbf{L}_w = 0.
\end{aligned} \tag{22}$$

□

D Reproducibility

Table 7: The statistics of datasets.

Dataset	Task	Nodes	Edges	Features	Classes
Cora	Transductive	2,708	5,429	1,433	7
Citeseer	Transductive	3,327	4,732	3,703	6
Pubmed	Transductive	19,717	44,338	500	3
Cora Full	Transductive	19,793	65,311	8,710	70
Ogbn-arxiv	Transductive	169,343	1,166,243	128	40

D.1 Datasets

Cora is a well-known citation network that is labelled by paper topic. The majority of approaches report on a subset of this dataset. The **Cora** dataset contains 2708 scientific publications divided into seven categories. The citation network has 5429 links. Each publication in the dataset is described by a 0/1-valued word vector indicating the absence/presence of the corresponding dictionary word. The dictionary contains 1433 distinct words. **Cora Full** is made up of 19793 scientific publications divided into seventy categories. The citation network has 65311 links. The dictionary contains 1433 distinct words.

CiteSeer contains 3312 scientific papers divided into six categories. The citation network has 4732 linkages. Each publication in the dataset is described by a 0/1-valued word vector indicating the absence/presence of the relevant dictionary word. The dictionary has 3703 distinct terms.

Pubmed is comprised of 19717 scientific papers on diabetes from the PubMed database, grouped into one of three categories. The citation network has 44338 linkages. Each publication in the dataset is described by a TF/IDF weighted word vector drawn from a vocabulary of 500 distinct terms.

Ogbn-arxiv is the citation network represented by a directed graph of all Computer Science (CS) arXiv papers indexed by MAG [69]. Each node represents an arXiv paper, and each directed edge indicates that one paper references another. Each paper includes a 128-dimensional feature vector generated by averaging the embeddings of words in the title and abstract. Individual word embeddings are produced by running the skip-gram model [68] over the MAG corpus.

E Implementation Details

GLEN is implemented in PyTorch.The propagation procedure is implemented with sparse-dense matrix multiplications. The codes of GCN, COLES-GCN, SGC, COLES-SGC, S^2GC and COLES-S^2GC are also implemented with PyTorch. The weight matrices of classifier are initialized with Glorot normal initializer. We employ Adam [66] to optimize parameters of the proposed methods and adopt early stopping to control the training epochs based on the validation loss. For all experiments, we use Adam to optimize Eq. 5 because our method does not have a closed-form solution as COLES does. All the experiments in this paper are conducted on a single NVIDIA GeForce RTX 1080 with 8 GB memory on a PC with Unbuntu 18.04. We use Python 3.7.3, PyTorch 1.10.0, and CUDA 10.2.

E.1 Hyperparameters

Tables 8 and 9 summarize hyperparameters. GLEN is not highly sensitive to different hyperparameters. The only hyperparameter for SGC and S ^{2}GC is the aggregation step K. As a result, we use $K = 8$ for the majority of benchmarks. Except for Ogbn-arxiv, all contrastive-based approaches use logistic regression as the classifier. It is worth noting that we do not modify any logistic regression parameters and instead use the default settings. Ogbn-arxiv exhibits non-linear feature characteristics because Bag-of-Words was used by the authors to form embeddings. As a result, the MLP classifier is chosen for GLEN-S^2GC on this dataset. We specifically preserve the MLP classifier configuration from the baseline. The learning rate for the MLP is 0.005 and the dropout rate is 0.4.

Table 8: The hyperparameters of datasets (node classification).

Dataset	Optimizer	K	lr	weight decay	Epoch	hidden size
Cora	Adam	8	1e-3	5e-4	20	512
Citeseer	Adam	8	1e-4	1e-4	80	512
Pubmed	Adam	8	2e-2	1e-5	40	256
Cora Full	Adam	2	1e-2	0	30	512
Ogbn-arxiv	Adam	10	1e-2	0	500	126

Table 9: The hyperparameters of datasets (node clustering).

Dataset	Optimizer	K	lr	weight decay	Epoch	hidden
Cora	Adam	8	1e-2	5e-4	1	512
Citeseer	Adam	8	1e-4	1e-4	30	512
Pubmed	Adam	8	2e-2	1e-5	40	256

F Limitation and Broader Impact

Although we propose a promising criterion to learn discriminant features, the rank difference problem is NP-hard. Choosing and especially solving high-quality surrogates to the rank difference of terms is still an unsolved optimization problem that requires a further work within the optimization community.

This paper discusses the design of feature space from a critical point of view. To this end, it proposes a novel generalized graph embedding framework which is very different compared to the traditional graph embedding frameworks (*e.g.*, Laplacian Eigenmaps, Linear Discriminant Analysis or Contrastive Laplacian Eigenmaps). The scope of this framework is not limited to graph embedding. GLEN can help many downstream works which require learning discriminant representation in an unsupervised manner to improve the performance of downstream tasks. Node classification, object category recognition, metric learning and other downstream tasks can accelerate downstream training thanks to GLEN. More importantly, GLEN-S^2GC is a lightweight energy-friendly network compared to heavy GCN-based GCL (see 'Scalability' section).

Regarding negative impacts, we are not aware of any. GCL is an unsupervised learning paradigm which, by itself, cannot lead to any negative impact.

G Additional Results

Comparison with other frameworks. Below we redefine Local Preserving Projection (LPP) [65] and Deep Spectral Clustering (DSC) [67] within the COLES and GLEN frameworks. All models below are based on the S^2GC backbone:

- DSC extends Deep Spectral Clustering Learning [67] by minimizing $\text{Tr}(f_\Theta(\mathbf{X})^\top \mathbf{L}_w f_\Theta(\mathbf{X}))$ where f_Θ is a two-layer neural network (MLP). Kindly note this is non-contrastive learning that only uses $\mathbf{L}_w$.
- LPP is an extension of Locality Preserving Projections [65] that learns an orthogonal linear projection by minimizing $\text{Tr}(\mathbf{U}\mathbf{X}^\top \mathbf{L}_w \mathbf{X}\mathbf{U}^\top))$. Notice this is non-contrastive learning that only uses $\mathbf{L}_w$.
- COLES-LPP is defined by us as minimizing $\text{Tr}(\mathbf{U}\mathbf{X}^\top \mathbf{L}_t \mathbf{X}\mathbf{U}^\top)) - \text{Tr}(\mathbf{U}\mathbf{X}^\top \mathbf{L}_w \mathbf{X}\mathbf{U}^\top))$.
- COLES-DSC minimizes $\text{Tr}(f_\Theta(\mathbf{X})^\top \mathbf{L}_t f_\Theta(\mathbf{X})) - \text{Tr}(f_\Theta(\mathbf{X})^\top \mathbf{L}_w f_\Theta(\mathbf{X}))$. Two MLP layers are added (as in the DSC model above) between the S^2GC backbone and the loss (some models [70, 71] precede S^2GC with an MLP). Their layer parameters are added to Θ.
- GLEN-LPP is defined as $\log\det(\mathbf{U}\mathbf{X}^\top \mathbf{L}_t \mathbf{X}\mathbf{U}^\top)) - \log\det(\mathbf{U}\mathbf{X}^\top \mathbf{L}_w \mathbf{X}\mathbf{U}^\top))$.
- GLEN $\log\det(f_\Theta(\mathbf{X})^\top \mathbf{L}_t f_\Theta(\mathbf{X})) - \log\det(f_\Theta(\mathbf{X})^\top \mathbf{L}_w f_\Theta(\mathbf{X}))$ also uses two MLP layers as in the DSC model.

Table 10 below shows the results.

Table 10: Mean classification accuracy (%) and the standard dev. over 50 random splits. Numbers of labeled samples per class are in parentheses. The best accuracy per column is in bold. Models are organized into semi-supervised, contrastive and unsupervised groups. OOM means out of memory.

Method	Cora		Citeseer		Pubmed		Cora Full	
	(5)	(20)	(5)	(20)	(5)	(20)	(5)	(20)
S^2GC	71.4±4.4	81.3±1.2	60.3±4.0	69.5±1.2	67.6±4.2	73.3±2.0	41.8±1.7	60.0±0.5
LPP	34.5±1.6	54.4±1.5	30.5±1.4	42.3±1.5	39.4±5.3	43.9±4.7	50.8±1.4	61.8±0.5
DSC	32.5±3.9	53.4±4.6	37.2±4.0	48.2±3.0	40.0±5.6	39.2±5.6	50.0±0.0	60.0±1.0
COLES-LPP	75.0±3.4	81.0±1.3	67.9±2.3	71.7±0.9	62.6±5.0	73.2±2.6	47.6±1.2	59.2±0.5
COLES-DSC	73.7±3.0	80.4±1.0	67.4±2.0	71.9±0.9	60.3±6.0	65.9±1.7	23.0±1.4	38.3±1.1
GLEN-LPP	75.3±3.6	82.6±1.2	65.9±2.7	71.5±1.0	68.9±3.9	78.4±2.1	51.4±1.4	62.0±0.6
GLEN-DSC	**78.2±2.4**	**83.0±1.0**	**69.1±2.1**	**72.3±0.9**	**70.6±3.9**	**80.1±1.9**	**53.0±1.5**	**62.6±0.5**

H Derivation of GLEN from the SampledNCE framework

COLES [72] extends Laplacian Eigenmaps:

$$\underset{\mathbf{Z},\ s.t.\Omega(\mathbf{Z})}{\arg\min}\ W_{ij}^{+} \|\mathbf{z}_i - \mathbf{z}_j\|_2^2, \tag{23}$$

where $\mathbf{Z} = [\mathbf{z}_1, \cdots, \mathbf{z}_n]$ and $\Omega(\mathbf{Z})$ are constraints (*i.e.*, orthogonality) by expanding the SampledNCE formulation:

$$\mathbb{E}_{i\sim p_d}\left[\mathbb{E}_{j\sim p_d(j|i)}[s_\Theta(z_i, z_j)] + \eta\, \mathbb{E}_{j'\sim p_n(j'|i)}[\tilde{s}_\Theta(z_i, z_{j'})]\right]. \tag{24}$$

Symbols p_n and p_d are negative and positive sampling distributions respectively. Moreover, $s_\Theta(v, u) = \log\exp(\mathbf{u}^\top \mathbf{v}) = \mathbf{u}^\top \mathbf{v}$ and $\tilde{s}_\Theta(v, u') = \log\exp(-\mathbf{u'}^\top \mathbf{v}) = -\mathbf{u'}^\top \mathbf{v}$ are similarity measures, whereas $\eta \geq 0$ controls the impact of negative sampling.

GLEN generalizes SampledNCE, a framework for contrastive learning with positive and negative sampling, which relies on two terms:

$$\mathbb{E}_{v\sim p_d(v)}\left[\mathbb{E}_{u\sim p_d(u|v)} s(\mathbf{u}, \mathbf{v})\right] \quad \text{and} \quad \eta\, \mathbb{E}_{v\sim p_d(v)}\left[\mathbb{E}_{u'\sim p_n(u'|v)} \tilde{s}(\mathbf{u}', \mathbf{v})\right]. \tag{25}$$

The above two terms are evaluated over two different distributions $u \sim p_d(u \mid v)$ (nodes u from the adjacency matrix) and $u' \sim p_n(u' \mid v)$ (nodes u' from random negative adjacency matrix).

Let us consider the positive sampling term (the negative sampling term can be expanded in the similar way). Let $p_d(v) = \frac{1}{\sqrt{D_{vv}}}$ and $p_d(u \mid v) = \frac{\hat{W}_{uv}}{\sqrt{D_{uu}}}$ where $\hat{\mathbf{W}}$ is an unnormalized adjacency matrix and $\mathbf{D}$ is its degree matrix. Let $\mathbf{W}$ be the degree normalized matrix. Notice u and v are indexes of embeddings $\mathbf{u}$ and $\mathbf{v}$. Let $s(\cdot)$ be defined as in COLES. Then:

$$\mathbb{E}_{v\sim p_d(v)}[\mathbb{E}_{u\sim p_d(u|v)}, s(\mathbf{u},\mathbf{v})] = \sum_{u,v} W_{uv}\, s(\mathbf{u},\mathbf{v}) = \sum_{i=1}^{m}\sum_{u,v} W_{uv} u_i v_i = \phi(\mathbf{Z}^\top \mathbf{W}\mathbf{Z}), \tag{26}$$

where $\phi(\cdot)$ is a pooling function, *i.e.*, $\phi(\mathbf{M}) = \text{Tr}(\mathbf{M})$ yields COLES:

$$\sum_{i=1}^{m}\sum_{j=1}^{m} \delta(i-j)\phi(\mathbf{z}_i^\top \mathbf{W}\mathbf{z}_j) = \sum_{i=1}^{m} \phi(\mathbf{z}_i^\top \mathbf{W}\mathbf{z}_i) \quad \text{if} \quad \mathbf{z}_i \perp \mathbf{z}_j \text{ for } i \neq j, \tag{27}$$

where $\mathbf{z}_i \perp \mathbf{z}_j$ imposes orthogonality constraints of Laplacian eigenmaps and $\delta(z) = 1$ if $z = 0$ and $\delta(z) = 0$ if $z \neq 0$. Finally, think that rows of $\mathbf{Z}$ contain all $\mathbf{u}$ (and $\mathbf{v}$).

We let the pooling operator $\phi(\cdot)$ operate on the entire spectrum under a general aggregation scheme. A very general operator is $\phi(\mathbf{M}) = \text{Rank}(\mathbf{M})$ from which we can recover the original trace (nuclear norm) of COLES or LogDet of GLEN, γ-nuclear, S_p, and Geman norm, respectively.

COLES uses the following expression based on SampledNCE:

$$\min_{\mathbf{Z}} \sum_{i,j} W_{ij}^{+} \|\mathbf{z}_i - \mathbf{z}_j\|_2^2 - \Big(\frac{\eta}{\kappa}\sum_{l=1}^{\kappa} W_{ij}^{l,-}\Big)\|\mathbf{z}_i - \mathbf{z}_j\|_2^2 = \max_{\mathbf{Z}} \text{Tr}(\mathbf{Z}^\top \mathbf{L}_t \mathbf{Z}) - \text{Tr}(\mathbf{Z}^\top \mathbf{L}_w \mathbf{Z}), \tag{28}$$

where $\mathbf{W}^{+}$ is a normalized adjacent matrix and $\mathbf{W}^{l,-}$ are κ normalized randomized k-regular graphs (adjacency matrices), while $\mathbf{L}_w$ and $\mathbf{L}_t$ are the corresponding Laplacian matrices.

Negative random sampling is represented by $\mathbf{W}^{-}$, *e.g.*, a randomized k-regular graph or several such graphs.

If we sample $\kappa \to \infty$ randomized k-regular graphs (adjacency matrices of size $n \times n$) (each row receives 1 with probability k/n), the expectation of randomized graph (adjacency matrix) is given as:

$$\mathbb{E}[\mathbf{W}^{-}] = \lim_{\kappa\to\infty} \frac{1}{\kappa}\sum_{l=1}^{\kappa} \mathbf{W}^{l,-} = \frac{k}{n}\mathbf{1}\mathbf{1}^\top, \tag{29}$$

which by itself is a fully-connected graph with the graph Laplacian matrix $\mathbf{L}_t = \mathbf{I} - \frac{k}{n}\mathbf{1}\mathbf{1}^\top$.

We simply set $k = 1$ to use 1-regular graphs for negative sampling so $\mathbf{L}_t = \mathbf{I} - \frac{1}{n}\mathbf{1}\mathbf{1}^\top$. Thus, our contrastive term is equivalent of the total scatter matrix $\mathbf{S}_t$ known from the Linear Discriminant Analysis, *i.e.*, $\mathbf{S}_t = \mathbf{Z}^\top(\mathbf{I} - \frac{1}{n}\mathbf{1}\mathbf{1}^\top)\mathbf{Z} = \mathbf{Z}^\top \mathbf{L}_t \mathbf{Z}$. The positive sampling is encoded by the graph adjacency matrix $\mathbf{L}_w$.

Thus, our GLEN is given as:

$$\arg\max_{\mathbf{Z}} \ \text{Rank}(\mathbf{Z}^\top \mathbf{L}_t \mathbf{Z}) - \text{Rank}(\mathbf{Z}^\top \mathbf{L}_w \mathbf{Z}). \tag{30}$$

More precisely, if $\mathbf{Z}$ is produced by an encoder, *i.e.*, $\mathbf{Z} = f_{\boldsymbol{\Theta}}(\mathbf{X})$ then we optimize the above problem w.r.t. $\boldsymbol{\Theta}$.

References

[65] Xiaofei He and Partha Niyogi. Locality preserving projections. *Advances in Neural Information Processing Systems*, 16(16):153–160, 2004.

[66] Diederik P Kingma and Jimmy Ba. Adam: A method for stochastic optimization. *arXiv preprint arXiv:1412.6980*, 2014.

[67] Marc T Law, Raquel Urtasun, and Richard S Zemel. Deep spectral clustering learning. In *International conference on machine learning*, pages 1985–1994. PMLR, 2017.

[68] Tomas Mikolov, Ilya Sutskever, Kai Chen, Gregory S Corrado, and Jeffrey Dean. Distributed representations of words and phrases and their compositionality. In *Advances in Neural Information Processing Systems*, 2013.

[69] Kuansan Wang, Zhihong Shen, Chiyuan Huang, Chieh-Han Wu, Yuxiao Dong, and Anshul Kanakia. Microsoft academic graph: When experts are not enough. *Quantitative Science Studies*, 1(1):396–413, 2020.

[70] Lei Wang and Piotr Koniusz. Temporal-viewpoint transportation plan for skeletal few-shot action recognition. *Asian Conference on Computer Vision*, 2022.

[71] Lei Wang and Piotr Koniusz. Uncertainty-DTW for time series and sequences. *European Conference on Computer Vision*, 2022.

[72] Hao Zhu, Ke Sun, and Piotr Koniusz. Contrastive laplacian eigenmaps. *Advances in Neural Information Processing Systems*, 34, 2021.